

# Aerodynamic Classification of Swept-Wing Ice Accretion

Jeff M. Diebold\*, Andy P. Broeren† and Michael B. Bragg‡

The continued design, certification and safe operation of swept-wing airplanes in icing conditions rely on the advancement of computational and experimental simulation methods for higher fidelity results over an increasing range of aircraft configurations and performance, and icing conditions. The current state-of-the-art in icing aerodynamics is mainly built upon a comprehensive understanding of two-dimensional geometries that does not currently exist for fundamentally three-dimensional geometries such as swept wings. The purpose of this report is to describe what is known of iced-swept-wing aerodynamics and to identify the type of research that is required to improve the current understanding. Following the method used in a previous review of iced-airfoil aerodynamics, this report proposes a classification of swept-wing ice accretion into four groups based upon unique flowfield attributes. These four groups are: ice roughness, horn ice, streamwise ice and spanwise-ridge ice. In the case of horn ice it is shown that a further subclassification of “nominally 3D” or “highly 3D” horn ice may be necessary. For all of the proposed ice-shape classifications, relatively little is known about the three-dimensional flowfield and even less about the effect of Reynolds number and Mach number on these flowfields. The classifications and supporting data presented in this report can serve as a starting point as new research explores swept-wing aerodynamics with ice shapes. As further results are available, it is expected that these classifications will need to be updated and revised.

## 1.0 INTRODUCTION

The formation of ice on lifting surfaces in flight presents a serious risk to aircraft safety as well as a multitude of scientific and engineering challenges. Investigations into the accretion of ice and the resulting aerodynamic penalties began as early as the 1940s, and the research conducted in the past several decades has led to a thorough, but far from complete, understanding of the effects of ice on airfoils. Lynch and Khodadoust<sup>1</sup> provide a review of the performance effects of ice on airfoils and straight wings, while Bragg et. al.<sup>2</sup> reviewed the flowfield characteristics that lead to the observed performance effects. In addition to reviewing the flowfield of iced airfoils, Bragg et. al.<sup>2</sup> proposed an ice shape classification system that was based on the unique flowfield features generated by the ice. The classifications proved to be very useful when conducting parametric studies of the aerodynamic effects of ice on airfoils.

Our understanding of iced airfoil aerodynamics has reached a level of maturity where we can begin trying to understand the complex effects of ice on highly three-dimensional swept wings. Swept wing icing presents significant challenges because the parameter space for the 3D wing case is much larger and more complex than for airfoils. In addition to airfoil geometry, ice-shape geometry, size and location, the 3D wing geometry must be considered. Here the airfoil and ice accretion can vary along the span and wing sweep angle, twist, taper, dihedral and aspect ratio must also be considered. As a result of this complexity, there are relatively few studies investigating the effects of ice on swept wing aerodynamics.

NASA, FAA, ONERA, the University of Illinois, Boeing and others are embarking on a research program with goals to improve our understanding and ability to model ice accretion and the resulting aerodynamic effect on full-scale, 3D swept wings. The purpose of this review is to provide the initial framework for improving our understanding of swept wing icing, by reviewing much of the previous aerodynamic research in the context of a proposed ice shape classification system, similar to that developed by Bragg et. al.<sup>2</sup> for airfoils, and identify areas where more research is required. The classification is based on the fundamental flow physics that are unique to the different ice geometries and are responsible for the measured aerodynamic effects. Similar to 2D case, the proposed classifications are: ice roughness, horn ice, streamwise ice and spanwise-ridge ice. On a swept wing, the horn ice accretion can be further classified as with scallops, incomplete scallops or no scallops. It will be shown that from an aerodynamic point of view it may be more appropriate to classify the horn ice as nominally 3D and highly 3D horn ice. This review will discuss each classification with a focus on the unique aerodynamic characteristics as they are

---

\* Graduate Research Assistant, Department of Aeronautical and Astronautical Engineering, Member AIAA

† Aerospace Engineer, NASA Glenn Research Center, Icing Branch, Associate Fellow AIAA

‡ Professor of Aerospace Engineering, Interim Dean of College of Engineering, Fellow AIAA

currently understood. An effort will be made to interpret aerodynamic performance in terms of key flowfield features and where appropriate comparisons to the 2D case will be made. It should be noted that experimental swept wing icing data are limited and the different ice shape classifications have not received equal attention in the literature. In addition, most of the swept wing icing experiments have been conducted at low Reynolds numbers, and Reynolds number and Mach number effects are unknown. When the ice-shape classifications for airfoils were developed there was a better understanding of the aerodynamics and flowfields than currently exists for 3D iced wings. Therefore, as research is conducted and the knowledgebase increases, the classifications will undoubtedly change and improve. This report is a modified and updated version of the work of Broeren, Diebold and Bragg.<sup>3</sup>

## 2.0 Aerodynamic Classification of Swept Wing Ice Accretion

The purpose of this section is to review the existing body of technical literature on iced-swept wing aerodynamics in the context of a classification method based upon fundamental flowfield characteristics. The classifications include roughness, horn ice, streamwise ice and spanwise ridge ice. The focus of the following discussion will be on how the ice affects the flowfield and the performance, the physical characteristics and mechanisms through which the ice forms will only be discussed briefly. Vargas provides an excellent historical and technical summary of swept wing ice accretion.<sup>4</sup> As mentioned above, not all classifications have received an equal amount of attention. Currently, roughness and horn ice shapes have been the subject of the most investigations while streamwise and spanwise ridge ice have not been studied in as much detail.

### 2.1 Ice Roughness

Ice roughness refers to surface roughness associated with the initial stages of in-flight ice accretion. Anderson and Shin<sup>5</sup> characterized roughness formation on airfoils and found that initially the leading-edge contains a smooth zone, a rough zone and a feather region. These same features are observed for swept wings, but for large sweep angles in both glaze and rime icing conditions it has been observed that the smooth zone may not form. Despite this difference, the characteristics of initial icing roughness on swept wings are fundamentally the same as for airfoils and straight wings. Icing roughness can be characterized by height, location, chordwise extent, concentration and shape.<sup>2</sup> It has been observed on airfoils<sup>6</sup> and swept wings<sup>4</sup> that the height of the ice roughness elements is generally greater than the local boundary layer thickness. Vargas<sup>4</sup> points out that the effects of roughness of this size on the boundary layer instabilities and transition are unknown. It is reasonable to assume that the local separated flowfield in the vicinity of the roughness elements is not fundamentally different than in the airfoil case. For this, Bragg et al.<sup>2</sup> provide a detailed review of the roughness flowfield including the relevant phenomenological features, effects on transition and turbulence and impact on aerodynamic performance. For swept wings, the questions that arise have to do with the interaction of this flowfield with the spanwise and vortex flows.

Fortunately, in the case of roughness there is a fair amount of experimental data in the literature from studies unrelated to icing. The National Advisory Committee for Aeronautics (NACA) has conducted numerous experimental investigations into the aerodynamics of swept-wing configurations. Many of the studies explored Reynolds and Mach number effects and included cases with carborundum grains applied to leading edges. Neely and Conner<sup>7</sup> investigated leading-edge roughness effects in the Langley 19-foot pressure tunnel on a full-span wing with aspect ratio 4, 42 deg. leading-edge sweep, mean aerodynamic chord = 34.71 inches, and taper ratio = 0.625. Aerodynamic testing was conducted over a Reynolds number range of  $1.7 \times 10^6$  to  $9.5 \times 10^6$  with corresponding Mach number range of 0.10 to 0.22. Flow visualization showed that the stall of the clean wing began with separated flow near the trailing-edge of the outboard sections and progressed forward and inboard on the wing. In contrast, with  $k/c_{mac} = 0.00032$  diameter carborundum grains applied between  $x/c = 0.08$  on the lower surface to  $x/c = 0.08$  on the upper surface covering approximately 5 to 10% of the area, flow separation began at the leading-edge outboard sections. The effect of Reynolds number and surface roughness on the lift and drag is shown in Figs. 1 and 2 respectively. It can be seen that for all Reynolds numbers, the application of leading-edge roughness reduced  $C_{L,max}$ , reduced the stalling angle of attack and increased the drag. In addition, the roughness reduced the effects of Reynolds number. All of these trends are typical of what has been observed in numerous airfoil studies with roughness.

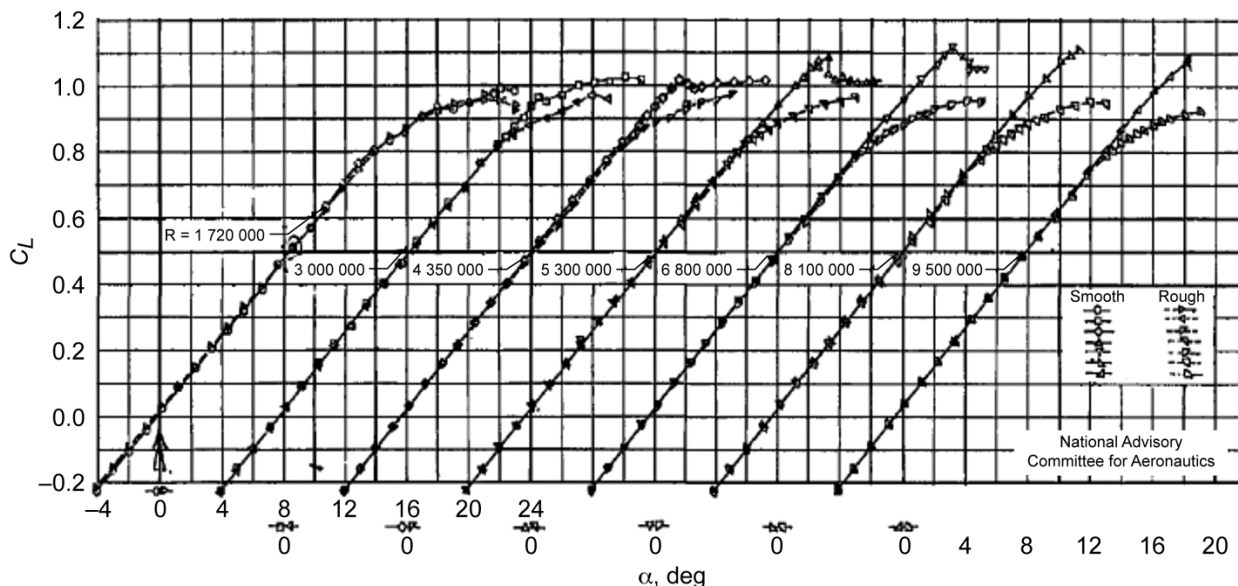
Kind and Lawrysyn<sup>8</sup> numerically investigated the effects of wing frost on a jet transport wing with an aspect ratio of 7.9, 30 deg. sweep and taper ratio of 0.25. Figure 3 shows the effects of roughness with  $k/c_{mac} = 0.00006$  on lift and drag for various chordwise extents of the roughness. The numbers in the figure legend indicate the chordwise extent of the roughness on the wing upper surface: "50" indicates the roughness extended from  $x/c = 0.42$  to the trailing edge, "75" indicates  $x/c = 0.20$  to the trailing edge, "95" indicates  $x/c = 0.009$  to the trailing edge and

“99” indicates  $x/c = 0.00$  to the trailing edge. Their results indicate that the roughness reduced both the slope of the lift curve and  $C_{Lmax}$  for all levels of coverage, but the wing was most sensitive to roughness located in the first 1% of the chord.

Papadakis et al.<sup>9</sup> performed an investigation of roughness on the leading edge of a business jet T-tail configuration. Sandpaper was used for the roughness with grit sizes of 40, 80, 120 and 180 covering from approximately  $x/c = 0.025$  on the lower surface to  $x/c = 0.016$  on the upper surface. The chordwise extent was determined from a droplet trajectory analysis. The horizontal tail had a leading-edge sweep of 29 deg., aspect ratio 4.4 and taper ratio of 0.43. A full-scale model was tested in the NASA Ames 40x80-ft wind tunnel and a 25% scale model was tested in the Walter H. Beech Memorial 7x10-ft tunnel. The full-scale model had a mean aerodynamic chord of 49.2 in. and the 25% scale model had a mean aerodynamic chord of 12.3 in. The 25% scale model was tested at a maximum Reynolds number of  $1.36 \times 10^6$ , where it was found that the 40 and 80 grit roughness ( $k/c_{mac} = 0.001375$  and  $0.000605$ ) reduced  $C_{Lmax}$  by 4.5% and 2.8% respectively; however, the 120 and 180 grit roughness ( $k/c_{mac} = 0.000365$  and  $0.000259$ ) increased  $C_{Lmax}$  by 4.9% and 1.9% respectively. Testing of the full-scale model at  $Re = 5.1 \times 10^6$  showed that the 40 and 120 grit roughness ( $k/c_{mac} = 0.000344$  and  $0.000091$ ) decreased  $C_{Lmax}$  by 18.5% and 15.9% respectively. Surface pressure measurements and boundary layer profile measurements at  $x/c = 0.6$  and  $2y/b = 0.51$  showed that the leading-edge roughness led to significantly thicker boundary layers and trailing-edge separation.

These results demonstrate the possible large aerodynamic penalties of roughness but also a potential problem of testing at low Reynolds numbers. Low Reynolds number experiments can mask the true penalties of ice shapes because the clean wing performance generally suffers as a result of the low Reynolds number more than the iced wing. In the 2D case, it has been shown that the Reynolds number typically has a substantially smaller effect on the iced airfoil aerodynamics than for the clean airfoil.<sup>2</sup> This is because the ice shape fixes the separation location thereby eliminating a potential mechanism through which the Reynolds number can affect performance. Therefore, while low Reynolds number experiments of iced airfoils are generally representative of higher Reynolds number, the low Reynolds number clean airfoil experiments may not and care must be taken when interpreting results. The low Reynolds number of the 25% scale experiments of Papadakis<sup>9</sup> may explain the increase in  $C_{Lmax}$  for the 120 and 180 grit roughness, because the classification of roughness does have the potential to depend more on the Reynolds number than other classifications.<sup>2</sup> It should be noted that due to the lack of high Reynolds number swept wing icing experiments, it is unknown how the Reynolds number effects iced swept wings.

While these roughness studies do provide some initial insights, more research is needed to understand the effect of size, location, concentration, Reynolds number and other factors important to the aerodynamics of iced-swept wings. There is very little or no flowfield information such as surface pressures, flow visualization and velocity profiles in these reports. An understanding of the roughness flowfield is important to accurate subscale simulation of roughness effects.



**Fig. 1 Effect of Reynolds number and leading-edge roughness on the lift coefficient of a 42 deg. leading-edge swept wing, after Neely and Conner.<sup>7</sup>**

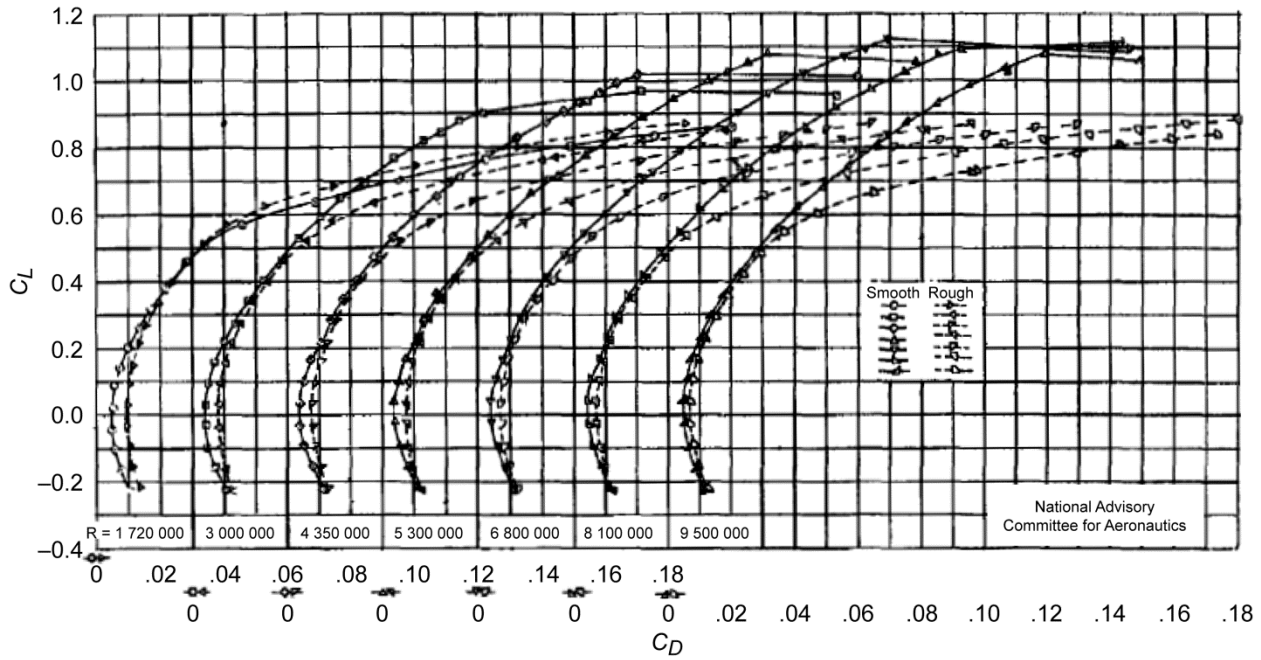


Fig. 2 Effect of Reynolds number and leading-edge roughness on the drag polar of a 42 deg. leading-edge swept wing, after Neely and Conner.<sup>7</sup>

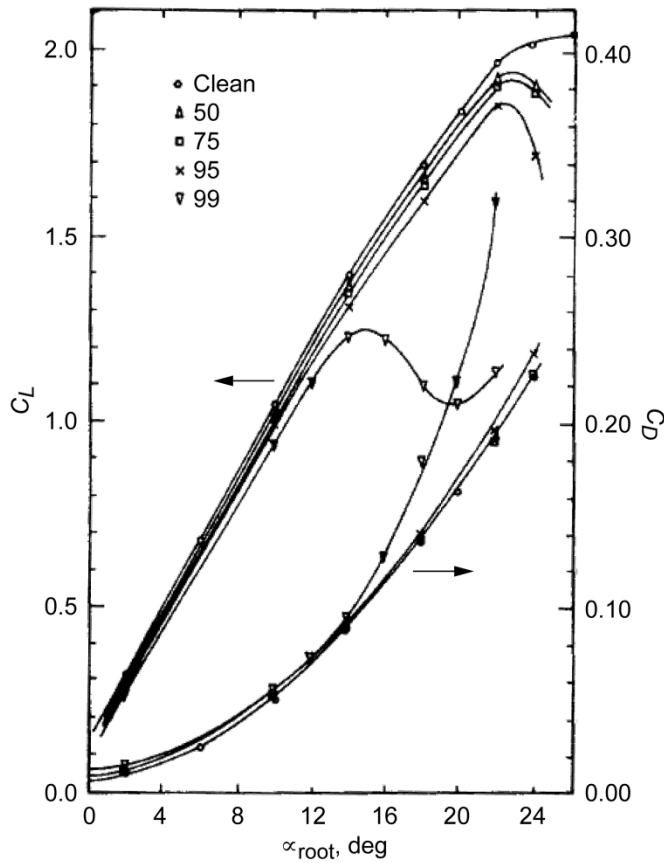
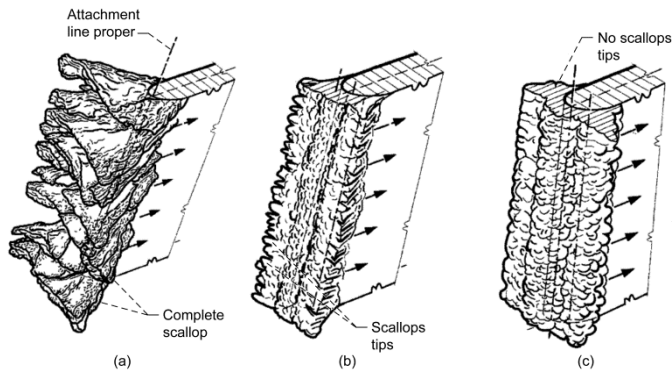


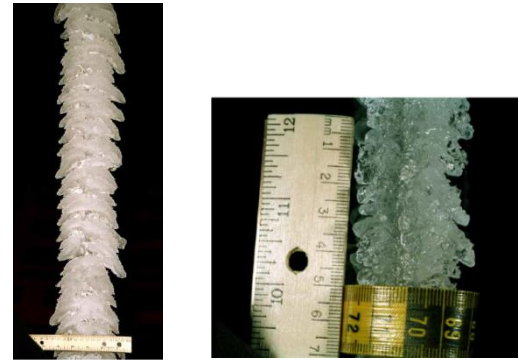
Fig. 3 Effect of simulated upper surface frost on a generic jet transport wing, after Kind and Lawrysyn.<sup>8</sup>

## 2.2 Horn Ice

On airfoils, glaze icing conditions often lead to leading-edge ice accretion known as horn ice. There are several geometric features that are important to the horn-ice shape, including height, the angle it makes with respect to the flow and its surface location.<sup>2</sup> For a swept wing in glaze or mixed icing conditions, ice accretion can be divided into three subcategories known as complete scallops, incomplete scallops and no scallops. An illustration<sup>4</sup> of each shape is shown in Fig. 4, and photographs<sup>10</sup> of a complete and incomplete scallop ice accretion are shown in Fig. 5. The type that forms has been found to be dependent on sweep angle and icing conditions.<sup>4</sup> Based on the aerodynamic classification system proposed here, the ice accretions in Fig. 4 can be classified as horn ice. It will be shown in this section that on swept wings a further subclassification of “nominally 3D” or “highly 3D” horn ice is necessary. These subclassifications are based on the fundamental aerodynamics of the particular ice shape which will be explained in this section. Based on available data, ice accretions with no scallops or incomplete scallops can be considered nominally 3D horn ice while accretions with full scallops can be considered highly 3D horn ice.



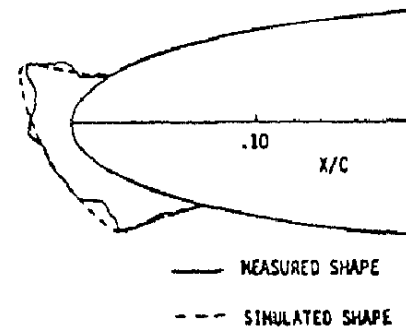
**Fig. 4 Ice accretion on a swept wing in glaze icing conditions. Arrows indicate direction of flow. a) Complete scallops, b) Incomplete scallops, c) No scallops.<sup>4</sup>**



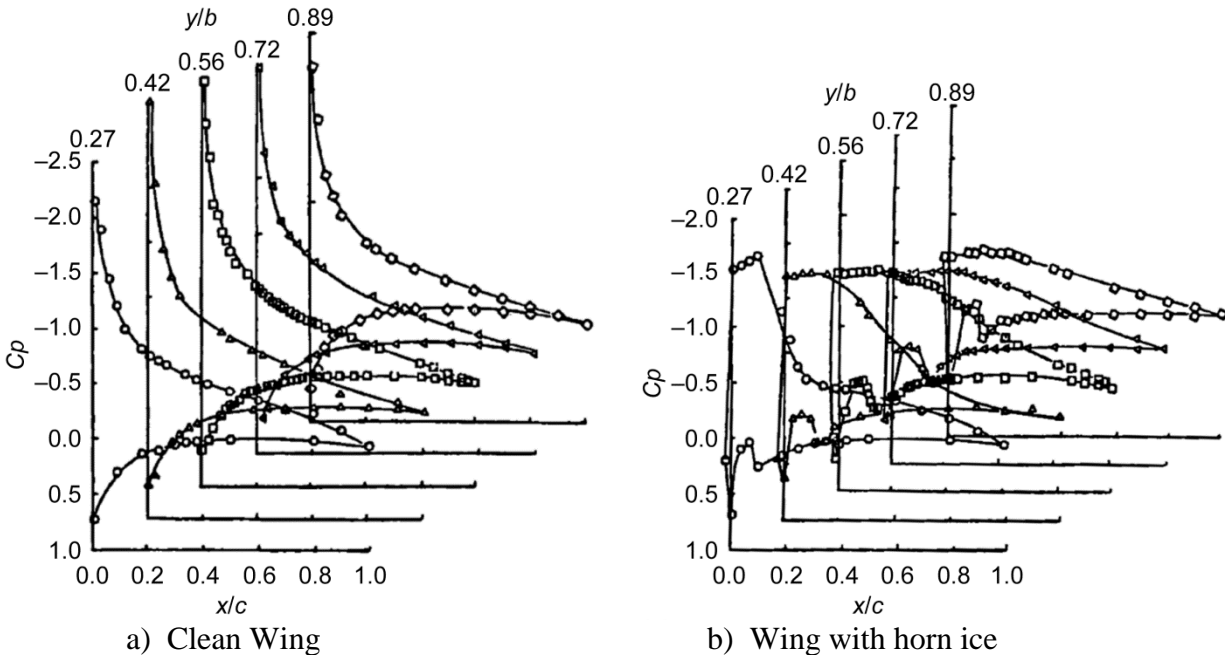
**Fig. 5 Photographs of complete and incomplete scallop glaze ice accreted on a wing having 28 deg. leading-edge sweep in the NASA Glenn Icing Research Tunnel.<sup>10</sup>**

In contrast to ice roughness on swept wings, there is some fundamental research regarding the flowfield about a 3D wing with horn ice. An early experimental study by Khodadoust and Bragg<sup>11</sup> and an accompanying CFD study by Kwon and Sankar<sup>12</sup> investigated the performance and flowfield of a semispan wing with a chord of 15-inches, sweep angle of 30 deg. and an aspect ratio of approximately 2.3. A NACA 0012 airfoil section was used. The ice shape used for the experiment and the CFD study was a simulation of a horn ice shape that was formed on a NACA 0012 airfoil in NASA’s IRT. Figure 6 shows the cross sections of the IRT generated ice shape and the simulated shape used for the experiment and the CFD study. The 2D cross section was extruded along the span and in the framework of the proposed aerodynamic classification system this ice shape is nominally 3D horn ice.

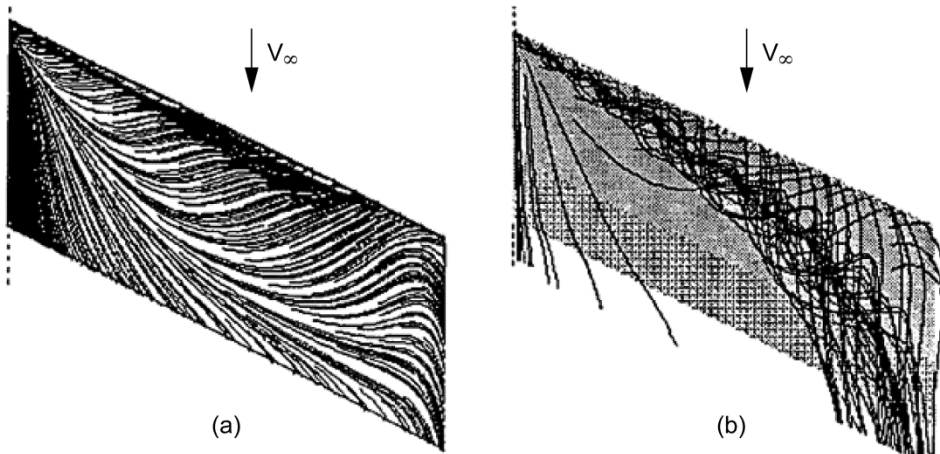
Figure 7 shows experimental pressure distributions at several spanwise locations with and without the horn ice at  $\alpha = 8^\circ$  and  $Re = 1.5 \times 10^6$ . The pressure distributions show that when the horn ice is present the leading-edge suction peaks are replaced by regions of nearly constant pressure covering approximately 20 to 40% of the chord. This is very similar to the pressure distribution on an airfoil with a horn shape where the pressure plateau indicates a separation bubble. In the case of a swept wing however, the separated flow and spanwise pressure gradient result in a three-dimensional leading-edge vortex. This vortex can clearly be seen in Fig. 8 which shows surface oil flow and a particle trajectory simulation from the CFD results for the iced wing at the same conditions as Fig. 7. The vortex grew in diameter moving outboard along the wing, and was lifted off the wing surface and shed into the wake near the tip. The effect of the increasing diameter of the vortex is seen in the broadening and reduction of the pressure peaks in Fig. 7. The simulated surface-oil flow showed regions of purely spanwise flow near the trailing edge and regions of almost completely reversed flow near the leading edge. These flowfield characteristics are analogous to the fundamental studies of swept wing stall conducted by Poll<sup>13</sup>.



**Fig. 6 Measured and simulated glaze ice shape.<sup>11,12</sup>**



**Fig. 7** Pressure distributions for the NACA 0012 swept wing with and without the horn ice shape,  $\alpha = 8^\circ$ ,  $Re = 1.5 \times 10^6$  after Bragg and Khodadoust.<sup>11</sup>



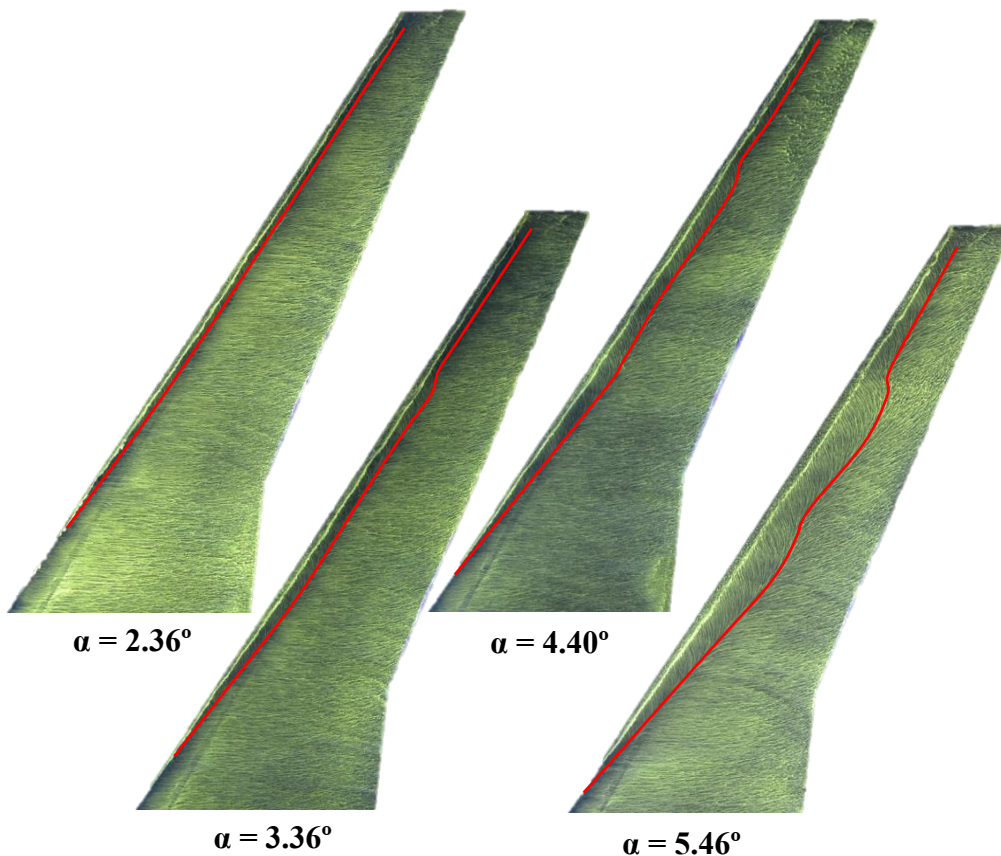
**Fig. 8** Flowfield over the NACA 0012 swept wing with horn ice shape: a) CFD surface oil simulation and b) CFD Particle trajectory simulation,  $\alpha = 8 \text{ deg.}$ ,  $Re = 1.5 \times 10^6$ , after Kwon and Sankar.<sup>12</sup>

Bragg et. al.<sup>14</sup> used LDV to study the flowfield of the same swept NACA 0012 wing used by Khodadoust<sup>11</sup> and Kwon<sup>12</sup>. The LDV was used to measure all three components of velocity at several spanwise locations for  $\alpha = 8^\circ$  and  $Re = 1.0 \times 10^6$ . Streamwise velocity measurements showed the inviscid flow accelerating over the ice shape leading to maximum values of  $u/U_\infty$  of 1.53 and 1.39 located at  $y/b = 0.4$  and  $y/b = 0.7$  respectively. Just downstream of the separation point, spanwise velocities of nearly twice the freestream velocity were measured. In general the velocities within vortex decreased as the tip was approached due to the increasing size of the vortex; however, near the tip large spanwise velocities due to the tip vortex were observed. Due to limitations of the experimental setup the only turbulence quantity obtained was  $\overline{u'^2}$ . Maximum turbulence intensities of nearly 35% were measured in the shear layer.

A more recent low-Reynolds number study by Diebold et. al.<sup>15</sup> investigated the performance and flowfield of a semispan wing with 35 deg. leading-edge sweep, an aspect ratio of 8.3, taper ratio of 0.296 and a mean aerodynamic



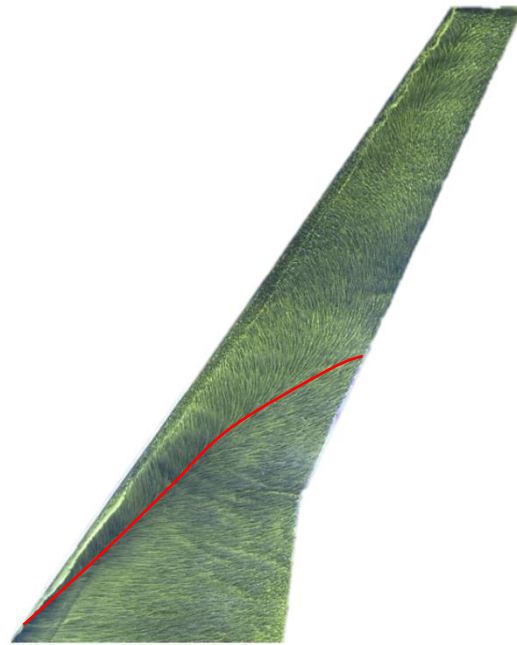
chord of 6.9-inches. A nominally 3D horn ice shape was used. The ice shape simulation was formed by lofting several 2D ice shape cross sections along the span. The model was based on the CRM, designed by Vassberg,<sup>16</sup> and was representative of a modern wide body commercial airliner. Experiments included force balance measurements, pressure sensitive paint, surface oil flow visualization and 5-hole probe wake surveys. Figure 9 shows oil flow images for the iced wing at several angles of attack for a Reynolds number of  $3 \times 10^5$ . The oil flow clearly indicates the presence of a leading-edge vortex. In Fig. 9, the reattachment line of the leading-edge vortex, which indicates where the separated shear layer has reattached to the surface, is highlighted. It can be seen that as the angle of attack increased, the reattachment line moved downstream indicating that the size of the leading-edge vortex grew. This is very similar to flowfield of an airfoil with a horn ice shape. As the angle of attack increases the separation bubble on the airfoil grows in the chordwise direction.<sup>2</sup> Pressure sensitive paint results on the swept wing indicated reduced pressure peaks and broad regions of nearly constant pressure under the vortex similar to Fig. 7b.



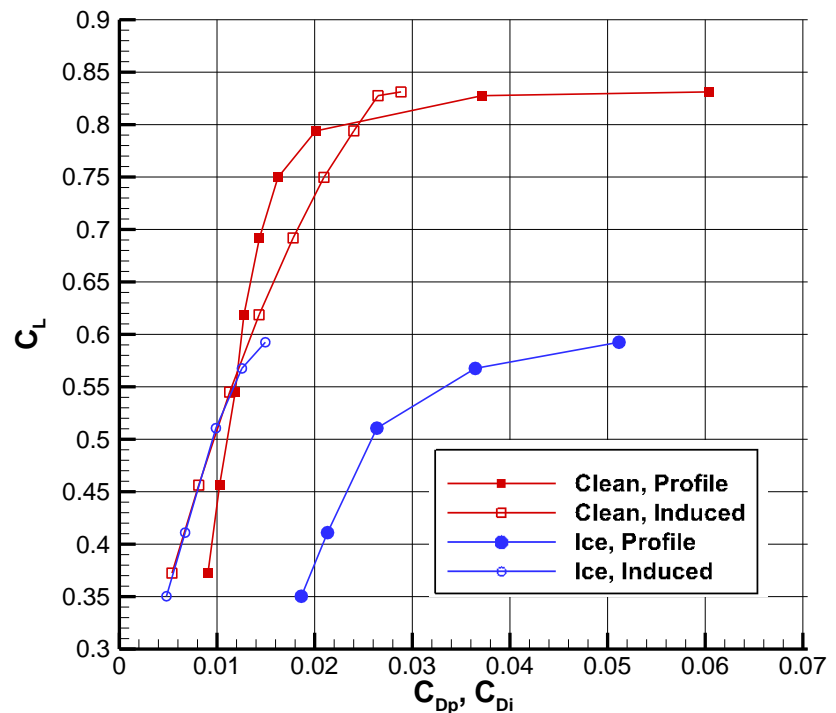
**Fig. 9** Reattachment line of the separated flow on the iced wing for a range of angles.  $Re = 3 \times 10^5$ . Adapted from Diebold et. al.<sup>15</sup>

When an airfoil with horn ice reaches the stalling angle of attack, the separated flow fails to reattach. When a swept wing with horn ice stalls the flowfield is far more complex than for an airfoil. Figure 10 shows the oil flow of the stalled swept wing with ice. On the inboard sections of the wing the separated shear layer was able to reattach to the surface and the flow is qualitatively similar to the flow at lower angles of attack. Over the outboard sections of the wing however, the separated shear layer was unable to reattach and this section of the wing was stalled. The leading-edge vortex began near the root and quickly turned downstream and was shed into the wake creating a similar flowfield to that of the swept NACA 0012 shown in Fig. 8.

Diebold and Bragg<sup>17</sup> studied the performance of the same swept wing model as Diebold et. al.<sup>15</sup> using a 5-hole probe wake survey analysis. Using methods described by Brune<sup>18</sup>, measurements of velocity and pressure in the wake were used to determine the lift and drag on the model, decompose drag into profile and induced drag components and measure the spanwise distribution of lift and drag. Figure 11 shows  $C_L$  of the clean and iced wing plotted against the profile and induced drag components. The wake survey results show that the increase in drag due to the ice shape is exclusively the result of an increase in the profile drag. For the same  $C_L$ , the ice shape does not affect the induced drag. The increase in profile drag due to the ice shape is a result of the large separated region behind the horn ice and the resulting pressure drag. In addition, the profile drag of the iced wing increased at much faster rate on the iced wing due to the increasing size of the leading-edge vortex which was seen in Fig. 9. The wake survey results of Diebold and Bragg<sup>17</sup> were also used to determine the spanwise distribution of lift and drag. Their results showed that for the particular ice shape and wing studied, the ice had a larger impact on the local aerodynamics of the outboard sections of the wing. This was explained as a result of a combination of the size of the ice shape relative to the local chord which increased as the tip was approached and the fundamental aerodynamics of swept wings. The spanwise flow on a swept wing acts as a form of boundary layer suction<sup>19</sup> which may have helped promote reattachment of the separated flow. Diebold and Bragg<sup>17</sup> were also able to relate features seen in the surface oil flow to features in the lift and drag distributions. It should be noted that the experiments of Diebold et. al. and Diebold and Bragg were conducted at very low Reynolds numbers ( $Re < 1 \times 10^6$ ) and it is unknown if the observations discussed here will hold at higher Reynolds number.



**Fig. 10 Stalled iced wing with reattachment line highlighted.  $\alpha = 6.5^\circ$ ,  $Re = 3 \times 10^5$ . Adapted from Diebold et. al.<sup>15</sup>**



**Fig. 11  $C_L$  vs. components of drag for clean and iced wing measured from wake survey.  $Re = 6 \times 10^5$ .<sup>17</sup>**



The studies discussed above provided valuable insight into the flowfield of a swept wing with a horn ice shape. To better understand the performance effects of horn ice on swept wings it is necessary to utilize different and more realistic ice shapes. Papadakis et al.<sup>20</sup> investigated the effect of horn ice shapes on the T-Tail used in the roughness study<sup>9</sup> discussed in Section 2.1. The model was a 25% scale business jet T-Tail with a 29 deg. leading-edge sweep, a mean aerodynamic chord of 12.31 inches and an aspect ratio of 4.4. The ice shapes tested were generated using LEWICE (LEWICE<sup>21</sup> is a computational tool that simulates ice growth on surfaces exposed to icing conditions.), and in addition two spoilers consisting of a spanwise flat plate protruding normal to the airfoil surface were also tested. Cross-sectional views of the ice shapes and spoilers are shown in Fig. 12. The ice-shape simulations were generated using the same atmospheric conditions but different simulation times, 9 minutes and 22 minutes. The spoilers were used to represent only the height of the horn on the suction surface. Two types of spoilers were used, for one type the height matched the LEWICE shape along the span while the other type of spoiler had a constant height equal to the maximum height of the ice shape. Note, the suction surface is the lower surface. In addition, the LEWICE ice shapes were tested with and without 24-grit ( $k/c_{mac} = 0.0024$ ) roughness was added.

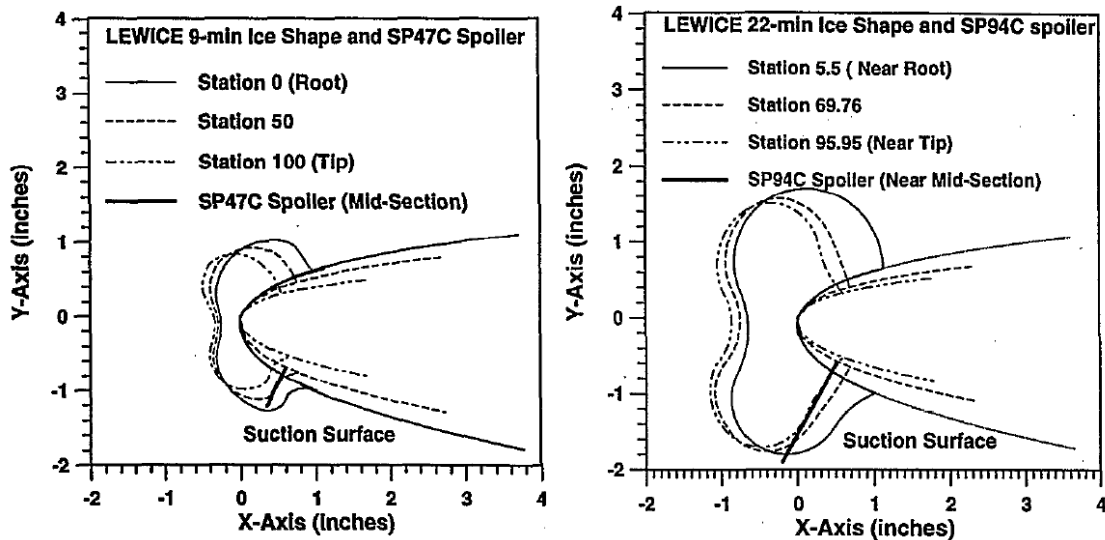


Fig. 12 Ice-shape simulations for 25% scale business jet T-Tail used by Papadakis et al.<sup>20</sup>

At a Reynolds number of  $1.36 \times 10^6$  the ice shapes had a significant effect on performance. The 9 minute and 22 minute LEWICE shapes reduced  $C_{L_{max}}$  10.8% and 24.5% respectively. The addition of 24 grit roughness reduced  $C_{L_{max}}$  by approximately 10% more than the corresponding smooth shapes. The addition of the roughness also increased the drag relative to the smooth shape. The large effect of added roughness, not typically seen in past airfoil studies, may be due to the aerodynamics of a swept wing; however, another potential explanation could be the geometry of the LEWICE simulations. The horns of LEWICE shapes are significantly more rounded than those of typical ice accretion. Because the horns are fairly rounded the point of separation may not be fixed to a specific location on the horn. Therefore, the addition of roughness may affect the separation location, whereas on a sharper horn this point would be fixed regardless of the surface condition. Surface pressure distributions showed that the roughness generally resulted in a reduced suction peak and a flatter broader  $C_p$  distribution, and boundary layer measurements near midspan at  $x/c = 0.6$  showed the application of roughness generally resulted in thicker boundary layers. Both of these observations support the idea that the roughness led to earlier separation on the ice shape.

When investigating the effects of ice on aerodynamic performance it is advantageous to use simple simulations for the ice shape. Several studies<sup>22,23</sup> have shown that very simple geometries, such as a leading-edge “spoiler,” can reproduce the performance characteristics of a horn-ice shape over a large angle of attack range. A simple geometry representing the height, angle, and location of the ice horn, essentially generates an equivalent separation bubble on the airfoil and, hence, very similar performance results. Figure 13 compares the lift of the smooth and rough LEWICE shapes, discussed above, with the constant and variable height flat plate spoilers. The designations L9 and L22 refer to the small and large smooth LEWICE shapes, and L9B and L22B refer to the same shapes with the 24 grit roughness added. The designations SP47C, SP47V, SP94C and SP94V refer to the spoilers. SP47 corresponds to the L9 ice shape and SP49 corresponds to the L22 ice shape. The C and V refer to constant height and variable

height respectively. Not unsurprisingly the spoiler with constant height, SP47C and SP94C had the largest effect because its height was equal to the maximum height of the ice shape and was constant along the span. Interestingly, the variable height spoilers, which matched the ice shapes height along the span, agreed well with the rough LEWICE shapes. It is perhaps surprising that the variable height spoiler matched the rough LEWICE shape as opposed to the smooth. This could possibly be because the location of the plate corresponds more closely to the separation point on the rough ice shape as opposed to the smooth shape; however, looking at surface pressure distributions and boundary layer measurements there are a few substantial differences between the rough LEWICE shape and the spoiler indicating the close match in performance may have been fortuitous. For example, pressure measurements at an angle of attack of  $-5^\circ$  showed poor agreement in both the magnitude of the suction peak and width of the separated region on the root and midspan sections.

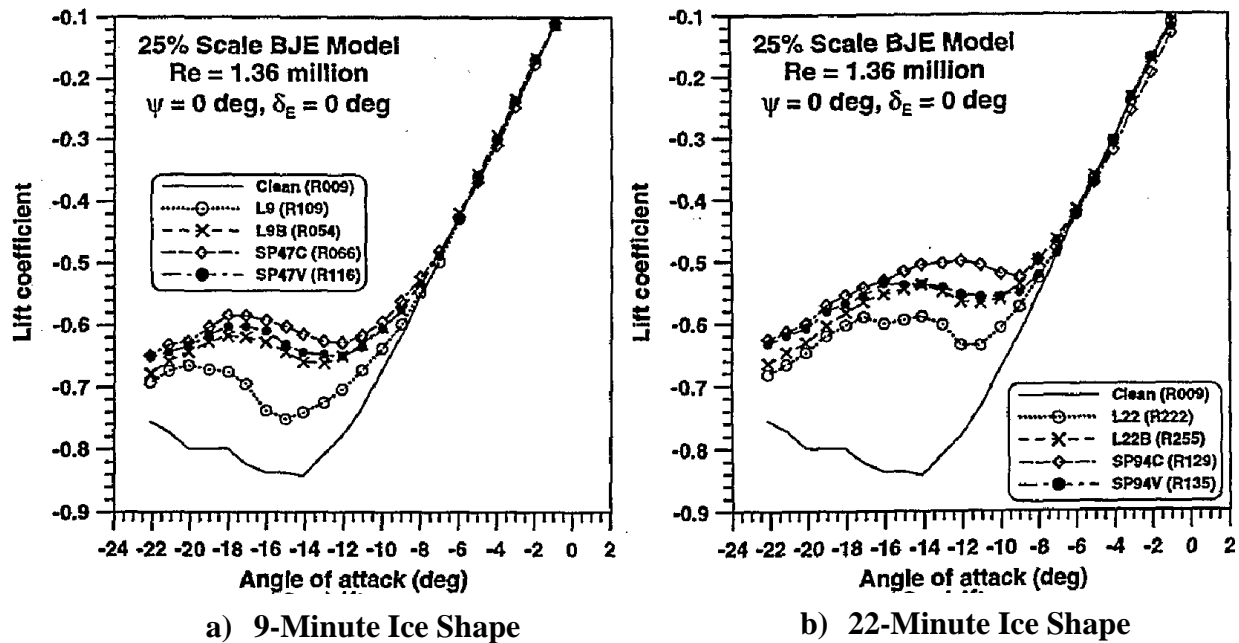
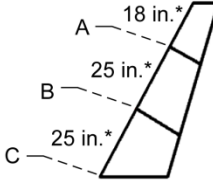
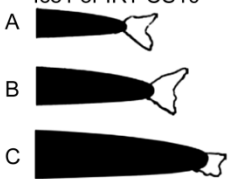
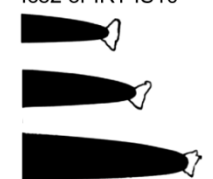

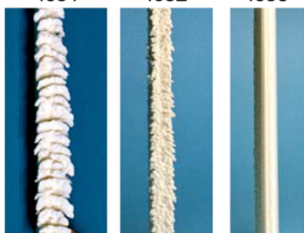



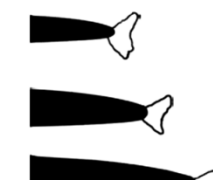


Fig. 13 Comparison of smooth and rough LEWICE shapes with constant and variable height flat plate spoilers for a) the 9-minute ice shape and b) the 22-minute ice shape.  $Re = 1.36 \times 10^6$ . Adapted from Papadakis et. al.<sup>20</sup>

The studies discussed above utilized ice shape simulations without any scallop features which can all be classified as nominally 3D horn ice. Studies by Papadakis et. al.<sup>24,25</sup> investigated the effects of several different ice shapes on a swept wing that included high-fidelity, three-dimensional ice-casting simulations incorporating various levels of incomplete and complete scallops. The swept-wing model had a GLC-305 airfoil section aligned in the streamwise direction with a 28 deg. leading-edge sweep, 18.72-inch mean aerodynamic chord, 60-inch semispan and an aspect ratio of 6.8. The ice shapes used for this study were formed on the same model in the NASA Glenn Icing Research Tunnel.<sup>10</sup> The icing conditions were chosen to produce a wide range of ice shapes including complete and incomplete scallops of various sizes and a rime ice formation. Moldings of the IRT ice accretions were subsequently used to produce the ice castings that were used for the aerodynamic tests. The ice-casting simulations captured the fully three-dimensional variation of the ice accretion.

The ice accretions tested and the corresponding tunnel conditions are shown in Table 1. Ice1 (IRT-CS10) is an example of a complete scallop glaze ice accretion. This shape can be compared with Ice2 (IRT-IS10) which is an example of an incomplete scallop. While the cross-sectional tracings look similar, the photographs reveal the large differences in the three dimensional geometry. Ice3 (IRT-SC5) is a rime ice accretion and will be discussed in Section 2.3. Ice4 (IRT-CS2) was formed at identical conditions to Ice1 (IRT-CS10), but with a much shorter exposure time of 2 minutes. Therefore, this is a relatively small glaze ice accretion and it is unclear if true scallop features formed due to the short exposure time. Ice5 (IRT-CS22) was also formed at identical conditions to Ice1 (IRT-CS10), but with a longer exposure time of 22.5 minutes. This longer duration led to the very larger complete scallop accretion shown in Table 1. Finally, Ice6 (IRT-IPSF22) had some characteristics of complete scallops that were not as fully developed as in Ice1 (IRT-CS10) and Ice5 (IRT-CS22).

**Table 1. Ice accretions and corresponding icing conditions used by Papadakis et al.<sup>24</sup>**

Ice1 or IRT-CS10	Ice2 or IRT-IS10	Ice3 or IRT-SC5	A = Normal to LE B = Normal to LE C = Streamwise 
 Complete scallops V = 250 mph AOA = 4° T <sub>total</sub> = 25 °F LWC = 0.68 g/m <sup>3</sup> MVD = 20 μm Time = 10 min	 Incomplete scallops V = 150 mph AOA = 4° T <sub>total</sub> = 25 °F LWC = 0.65 g/m <sup>3</sup> MVD = 20 μm Time = 10 min	 No scallops V = 201 mph AOA = 6° T <sub>total</sub> = 11.7 °F LWC = 0.51 g/m <sup>3</sup> MVD = 14.5 μm Time = 5 min	 
 Initial formation of scallops V = 250 mph AOA = 4° T <sub>total</sub> = 25 °F LWC = 0.68 g/m <sup>3</sup> MVD = 20 μm Time = 2 min	 Complete scallops V = 250 mph AOA = 4° T <sub>total</sub> = 25 °F LWC = 0.68 g/m <sup>3</sup> MVD = 20 μm Time = 22.5 min	 IPS failure case V = 150 mph AOA = 4° T <sub>total</sub> = 27 °F LWC = 0.46 g/m <sup>3</sup> MVD = 20 μm Time = 22.5 min	

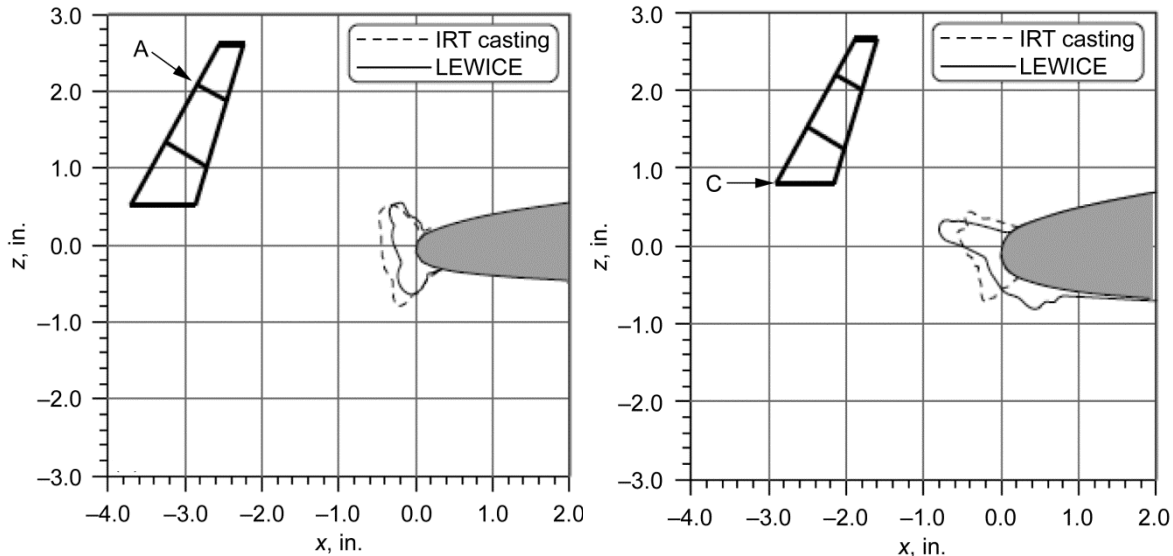
\*Distances are measured along wing leading edge, section C is at wing root, section B is 25-in. from wing root, section A is 50 in. from wing root or 18 in. from wing tip.

In addition to the IRT ice accretion in Table 1, seven additional ice shapes were generated using the ice accretion code LEWICE 2.0. Since LEWICE 2.0 is a 2D ice accretion code, the 3D simulations used for the aerodynamic testing were composed of 2D slices at several spanwise sections of the wing blended together. The detailed procedure is discussed in the original reference.<sup>24</sup> The LEWICE shapes were formed at the same conditions shown in Table 1, but the velocity and airfoil geometry used in the computations was the velocity normal to the leading edge. The LEWICE shapes did not contain any scallop features and as will be shown below can be classified as nominally 3D horn ice. These are designated with the prefix “LS” in the following figures. The geometry did vary in the spanwise direction but only according to the number of slices used to loft the 3D geometry. The effect of ice-shape roughness was also investigated by adding 36-grit size roughness ( $k/c_{mac} = 0.0011$ ) to the smooth LEWICE shapes.

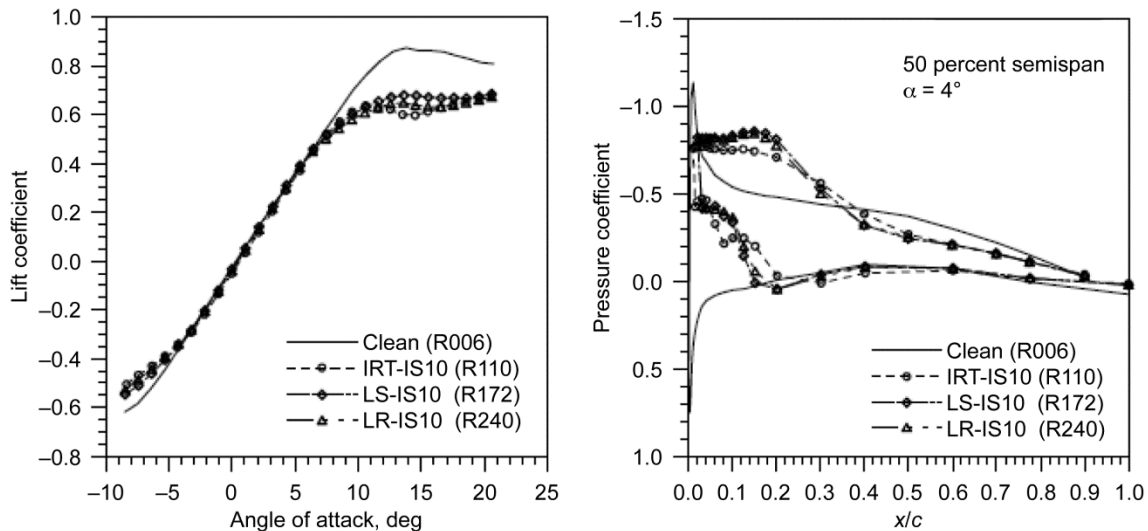
Because the Papadakis et al.<sup>24,25</sup> study utilized high-fidelity ice-casting simulations of the 3D ice accretions, it is possible to make some observations about the attendant aerodynamic effects relative to nominally 3D horn ice with minimal 3D features. Figure 14 shows a comparison of the ice accretion cross-section and the corresponding LEWICE shape for Ice2 (IRT-IS10) both of which can be classified as nominally 3D horn ice. Overall, there is reasonable agreement in the tracings, particularly for station A. Figure 15 compares the lift and  $C_p$  distributions for the IRT generated shape and the smooth and rough LEWICE shapes. The results here are very similar to what has been reported for horn ice simulations on airfoils.<sup>22</sup> The effect on lift coefficient is very similar for all three configurations up to the stall region where the 3D ice casting configuration has slightly lower maximum lift and stalling angle. For horn ice shapes on airfoils, small differences in the horn height, location or angle can significantly affect  $C_{L,max}$  and may explain the differences given the obvious differences in the cross sections shown in Fig. 14. The smooth LEWICE (LS-IS10) shape had slightly higher  $C_{L,max}$  than the LEWICE shape with roughness (LS-IS10), which is consistent with the observations for the business jet T-tail<sup>20</sup> discussed above and for past research on airfoils.

Also included in Fig. 15 is a comparison of surface pressure at the 50% semispan stations at  $\alpha = 4$  deg. For all three configurations, there are fairly well defined regions of approximately constant pressure from  $x/c \approx 0.0$  to  $x/c \approx$

0.2 on the upper surface. This pressure signature is similar to that shown previously in Fig. 7 due to the leading-edge vortex induced by the horn geometry. In their report, Papadakis et al.<sup>25</sup> provide more pressure comparisons at several angles of attack and for two additional spanwise locations. In most of these plots, the general shape of the distributions for the Ice2 (IRT-IS10) casting is similar to that for the LEWICE simulations. Thus indicating that for incomplete scallops, the large flowfield features (such as the leading-edge vortex) are similar to ice shape with no scallops described earlier in this section. Therefore, from an aerodynamic perspective, shapes with no scallops and incomplete scallops fall under the same classification of nominally 3D horn ice.



**Fig. 14 Comparison of IRT Ice2 (IRT-IS10) and LEWICE ice-shape cross sections on GLC-305 swept wing, after Papadakis et al.<sup>24</sup>**

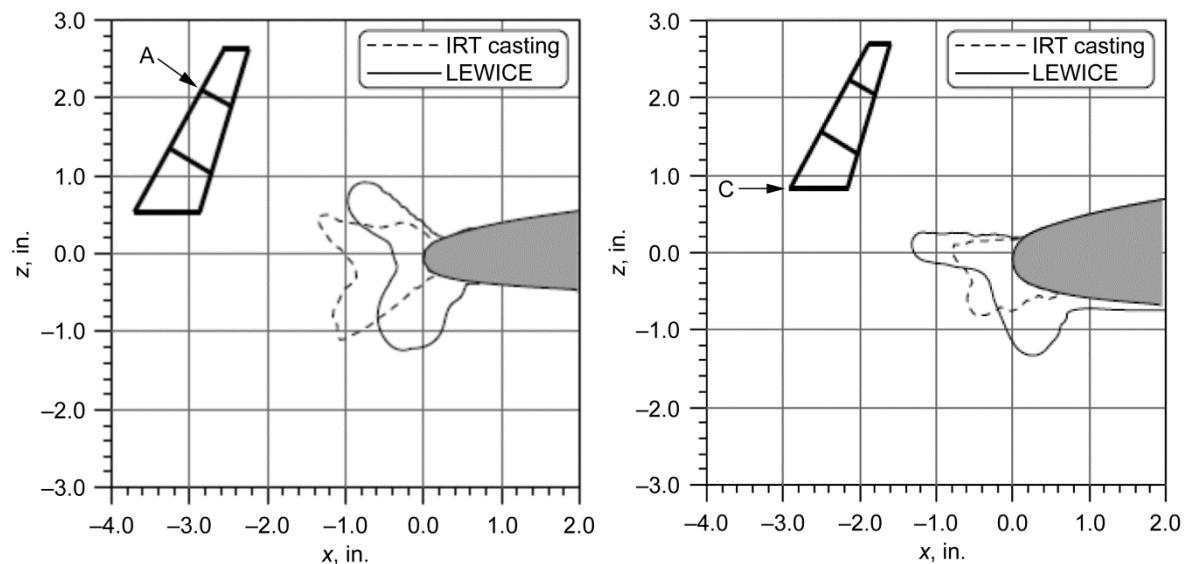


**Fig. 15 Aerodynamic effect of IRT Ice2 (IRT-IS10) and LEWICE ice-shape simulations on GLC-305 swept wing at  $Re = 1.8 \times 10^6$ , after Papadakis et al.<sup>24</sup>**

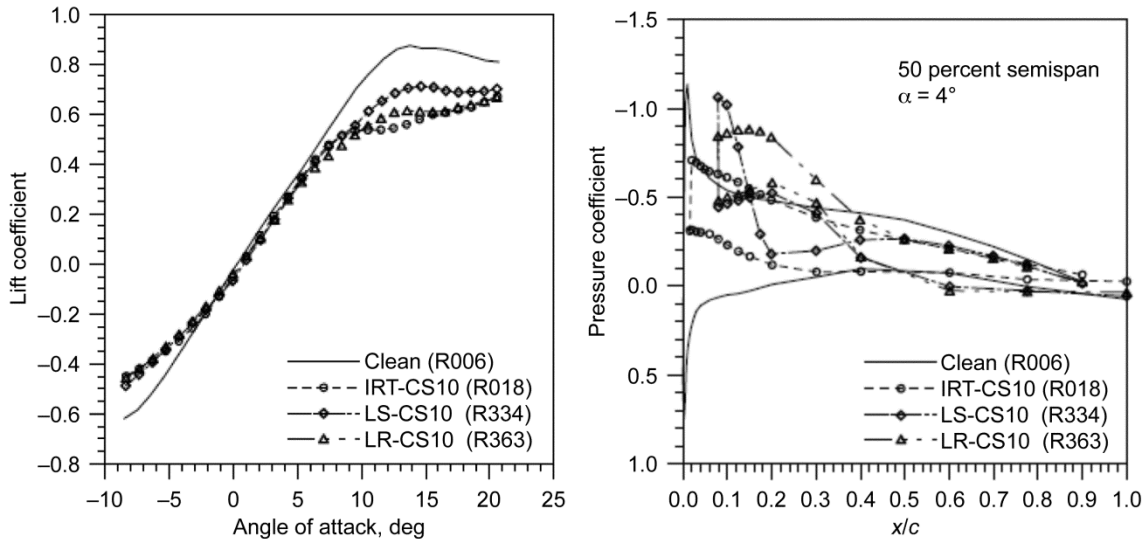
The data presented in Figs. 14 and 15 for the incomplete scallop configuration of Ice2 (IRT-IS10) are contrasted with the data for the complete scallop configuration of Ice1 (IRT-CS10). The cross-section geometry and LEWICE results are depicted in Fig. 16 where there are much larger differences in the two geometries relative to that shown in Fig. 14. This is most likely a result of the much higher degree of three-dimensionality associated with the complete scallop condition. It is not expected that the LEWICE cross sections in Fig. 16 should match since LEWICE does not generate 3D results. Even the most sophisticated ice accretion simulation codes do not predict the level of three dimensionality associated with a complete scallop ice accretion. It is also very difficult to compare a 2D tracing of a

highly 3D ice accretion as small changes in spanwise location can have a very large effect on the cross-sectional tracing.

Given these differences in geometry, it is interesting to compare the aerodynamic results in Fig. 17. For example, the main effect on lift coefficient is not observed until the stall region where the differences in  $C_{L,max}$  among the three configurations is larger than for the incomplete scallop case in Fig. 15. The selected pressure distribution shown in Fig. 17 is typical of the others plotted by Papadakis et al.<sup>24,25</sup> In this case, there is a sharp contrast between the pressure signatures of the Ice1 (IRT-CS10) casting and the LEWICE ice-shape simulations. The upper-surface pressure distribution of the LEWICE configurations are very similar to what has been shown previously in Figs. 7 and 15. This is particularly true for the case with roughness, LR-CS10. But for the Ice1 (IRT-CS10) casting, there is a gradual pressure recovery region with peak values of suction pressure much less than for the LEWICE shapes. A similar trend was observed for Ice6 (IRT-IPSF22) which also had a highly 3D ice accretion geometry typical of complete scallops. Since there are significant differences in cross-section geometries between the ice castings and the LEWICE simulations for Ice1 and Ice6 (not shown), better matching of the surface pressure distributions is not expected. What is of interest here is that the shape of the pressure distributions is different in the area immediately downstream of the ice shape. For the nominally 3D LEWICE shapes, there is a fairly distinct region of approximately constant pressure that has been shown to correspond to the leading-edge vortex. For the highly 3D geometry of the complete scallop ice casting simulation, this pressure region was not observed and the peak suction pressures were much lower. To the authors' knowledge, the flowfield immediately downstream of the highly 3D geometry has not been characterized or reported in the technical literature. These pressure data suggest that there exists a significantly different flowfield than for the nominally 3D horn ice shapes reported in other swept-wing icing studies. Papadakis et al.<sup>24</sup> suggest that the gaps between the scallop peaks allow high pressure air from the front face of the ice shape to leak through to the low pressure region behind the ice shape and alter the pressure distribution. Since current state-of-the-art ice accretion simulation codes are unable to predict highly three-dimensional features such as complete scallops, it is important to understand their impact on the aerodynamics. More research is needed to understand the flowfield associated with highly three-dimensional horn ice on swept wings so that the resulting impacts on wing performance may be better explained.



**Fig. 16 Comparison of IRT Ice1 (IRT-CS10) and LEWICE ice-shape cross sections on GLC-305 swept wing, after Papadakis et al.<sup>24</sup>**



**Fig. 17 Aerodynamic effect of IRT Ice1 (IRT-CS10) and LEWICE ice-shape simulations on GLC-305 swept wing at  $Re = 1.8 \times 10^6$ , after Papadakis et al.<sup>24</sup>**

Unlike the situation for other ice accretion on swept wings, there are currently both experimental performance measurements as well as flowfield studies for horn ice; although these studies offer valuable insights into the effect of horn ice accretions on swept wings there is still a substantial lack of information relative to the airfoil case. For example, a shortcoming of the studies discussed in this section is that no attempt was made to ensure that the IRT generated ice shapes were accurate representations of full-scale ice accretion. Other areas where experimental data are needed include more flowfield studies for detailed ice shapes with and without scallops and different wing geometries, parametric studies investigating geometrical features of the ice such as height, shape (e.g., tip radius, roughness level), location and the influence of wing geometry.

The data presented in this section for horn ice on swept wings suggest an aerodynamic subclassification that distinguishes between “nominally 3D” horn ice and “highly 3D” horn ice. Nominally 3D horn ice is associated with glaze ice accretion having either no scallops or incomplete scallops. This is only nominally 3D since the gross shape does not vary significantly over small spanwise distances. Highly 3D horn ice is associated with glaze ice accretion having complete scallops. In this case, the ice geometry changes significantly over small spanwise distances. From the perspective of aerodynamic classification, the difference between nominally 3D and highly 3D horn ice is defined in terms of the flowfield characteristics. The results discussed in this section for Figs. 7-15 were all associated with nominally 3D horn ice as there was very little change in the simulated ice geometry in the spanwise direction. The flowfield was described in terms of the leading-edge vortex and the resulting region of approximately constant surface pressure aft of the ice shape. This was contrasted against some results for highly 3D horn ice in Figs. 16 and 17 where the pressure signatures exhibited more gradual pressure recovery in place of the constant pressure regions aft of the ice shape. Due to a lack of data for highly 3D horn ice on a swept wing, the key flowfield characteristics in this case are unknown. To further distinguish between nominally 3D and highly 3D horn ice flowfield characteristics is yet another area where further research is required.

### 2.3 Streamwise Ice

This section will briefly discuss the classification of streamwise ice which is most often associated with rime icing conditions.<sup>2</sup> They typically follow the wing leading edge contour or form a horn-like shape, or protuberance, oriented into the flow direction. The available literature on this classification is very sparse. Papadakis et al.<sup>24</sup> tested one ice shape that could be classified as streamwise, Ice3 in Table 1. Figure 18 shows the effect of the IRT generated streamwise ice (IRT-SC5) as well as the smooth and rough LEWICE shapes. Although not shown here, for this particular case LEWICE predicted the ice shape very well. It can be seen that the IRT shape as well as both LEWICE shapes increased  $C_{L,max}$ . An increase in the maximum lift due to a streamwise ice shape has been observed on airfoils<sup>26</sup> and has been attributed to the ice shape effectively forming a leading-edge flap with the increase in



chord length and wing area relative to the reference area. Another potential factor may be the low Reynolds number at which the experiments were performed.

There is clearly a need for more aerodynamic data for streamwise ice on swept wings. It is expected that streamwise ice will not improve maximum lift performance in most cases. More information about the flowfield is required to understand the effects of roughness on streamwise ice that are thought to be important to the aerodynamics. For streamwise ice on airfoils, the aerodynamic effects were chiefly made manifest through trailing-edge separations. While small leading-edge separation bubbles were often observed at the ice/airfoil juncture this flowfield feature did not play a decisive role in the resulting aerodynamics. For swept wings, it is expected that this separation, if present, may lead to leading-edge vortex formation. It remains to be determined which of these effects, or perhaps both, contribute to the observed performance changes on the iced swept wing.

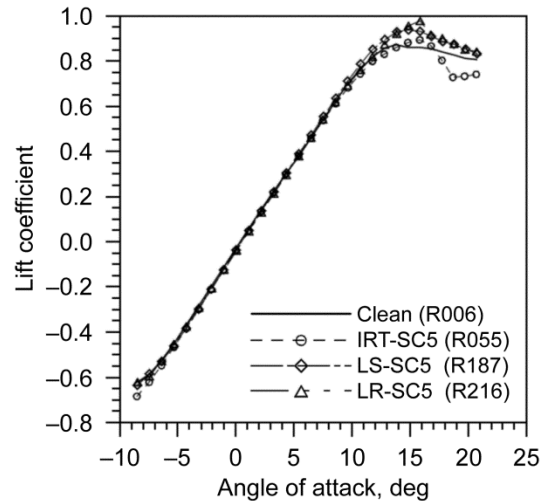


Fig. 18 Effect of streamwise ice on lift.  $Re = 1.8 \times 10^6$ . Adapted from Papadakis et. al.<sup>24</sup>

## 2.4 Spanwise Ridge Ice

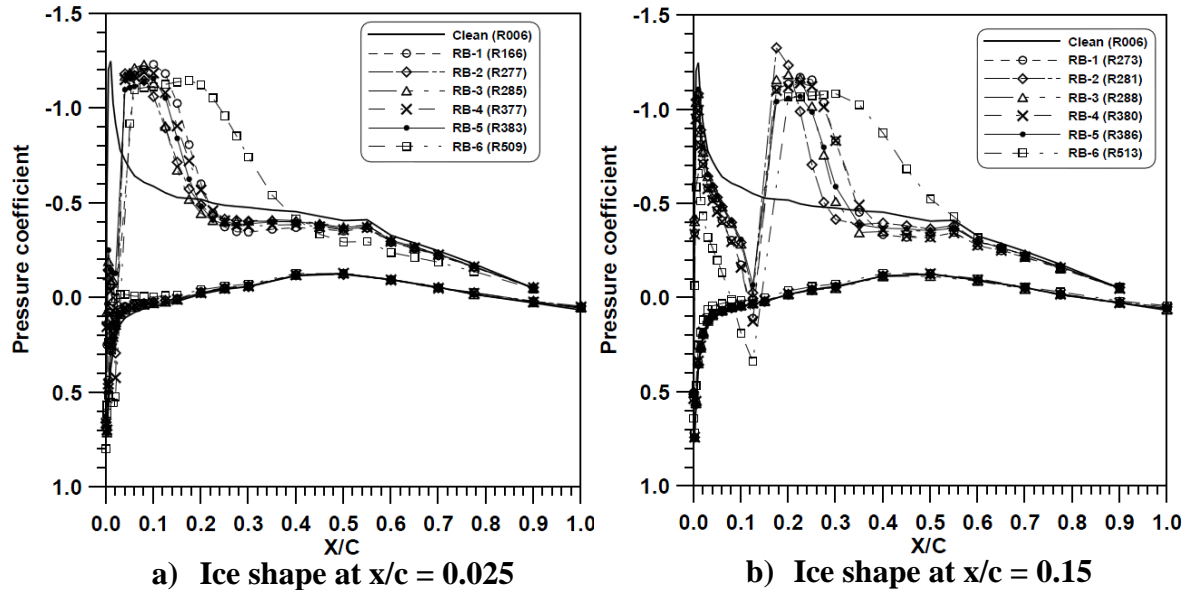
Spanwise-ridge ice can be associated with a number of icing conditions where the wing leading edge is free of ice with sometimes large ice formations located farther downstream. Typical examples are SLD icing conditions coupled with ice-protection system operation. Large drops can impinge on the wing aft of the protected areas sometimes forming an ice accretion best described as a ridge. Spanwise-ridge ice can also form when a heated leading-edge, ice-protected surface is not evaporating all of the impinging water. The liquid water flows downstream from the ice-protection system where it freezes forming a ridge oriented in the spanwise direction.

Like streamwise ice, there is very little available data on spanwise ridge ice. Papadakis et al.<sup>27</sup> performed a parametric study of spanwise-ridge ice on the same, swept GLC-305 model used by Papadakis et al.<sup>24</sup> Ice shapes were simulated by uniformly extending the simple geometries, shown in Table 2, across the span of the wing. The method of simulating spanwise-ridge ice with simple geometries is common practice for airfoils.<sup>28</sup> It is unknown if any effort was made to use simulations that accurately represented any documented full-scale ice accretion. The ridge heights ranged from 0.2 to 0.5-inches corresponding to 1% to 2.7% of the 18.72-inch mean aerodynamic chord. Each ice-shape simulation was tested at 2.5%, 5%, 10%, 15%, 20% and 30% chord measured in the streamwise direction. The effect of ridge size could be assessed by comparing performance measurements for the ice simulation RB-2 and RB-6 which showed that for a given chordwise location the larger ridge had a more significant impact. The importance of ridge shape could be observed by comparing results for RB-4 and RB-5 which showed that RB-4, with the flat surface facing forward, resulted in lower  $C_{L,max}$  and higher drag than RB-5, with the round surface facing forward. Similar results were observed in parametric studies of spanwise ridge ice on airfoils.<sup>29</sup> These parametric studies with airfoils showed that the chordwise location of the ridge was very important, and that the most severe penalties occurred when the ridge was located in a region of strong adverse pressure gradient.<sup>2,29</sup> In their test, Papadakis et. al.<sup>27</sup> observed that a given spanwise ridge simulation had the largest effect when it was located at 2.5% of the chord. Figure 19 shows the effect of all six simulated spanwise ridge shapes on

Table 2 Simulations of spanwise ridge ice used by Papadakis.<sup>27</sup>

Ice shape configurations	Dimensions	Flow direction
RB-1	0.2 in. (5 mm)  0.28 in. (7 mm)	
RB-2	0.25 in. (6.35 mm)  0.25 in. (6.35 mm)	
RB-3	0.2 in. (5 mm)  0.2 in. (5 mm)	
RB-4	0.25 in. (6.35 mm)  0.25 in. (6.35 mm)	
RB-5	0.25 in. (6.35 mm)  0.25 in. (6.35 mm)	
RB-6	0.5 in. (12.7 mm)  0.5 in. (12.7 mm)	

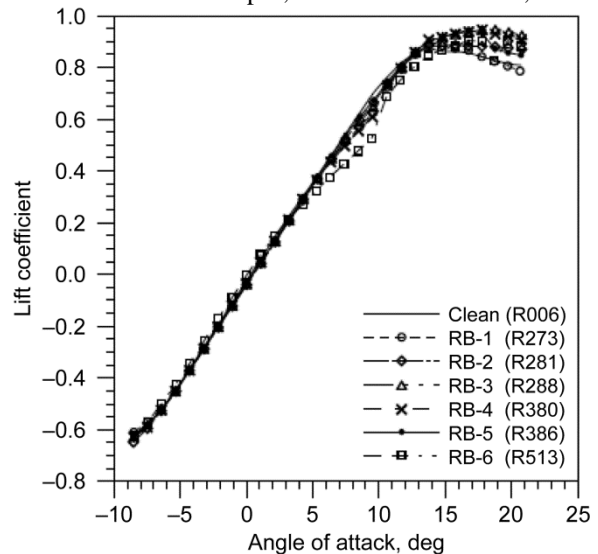
the pressure distribution at 15% semispan of the wing for two different locations of the ice shapes, 2.5% and 15%. The angle of attack was  $4^\circ$  and the Reynolds number  $1.8 \times 10^6$ . It can be seen that the suction peak of the clean wing was located at approximately 1% of the chord and therefore the spanwise ridge at 2.5% was located in a region of severe adverse pressure gradient. Figure 19a shows that when the ice shape was located at 2.5% it prevented the formation of the initial suction peak. The suction peak observed in the figure is due to the flow accelerating over the ice shape rather than around the leading edge. In contrast, Fig. 19b shows that when the ice shape was located at 15% the leading-edge suction peak was able to form which resulted in increased lift. Very similar results were observed by Lee and Bragg<sup>29</sup> during their experiments with spanwise ridges on airfoils.



**Fig. 19 Effect of different spanwise ridge ice simulations on pressure distribution at 15% span of GLC-305 swept wing at  $\alpha = 4^\circ$  and  $Re = 1.8 \times 10^6$ . Ice shape located at a) 2.5% and b) 15% chord. Adapted from Papadakis et. al.<sup>27</sup>**

All of the ice shapes tested by Papadakis et. al.<sup>27</sup> resulted in reduced lift curve slopes and increased drag regardless of the chordwise location; however, for most of the ice shapes and locations tested the maximum lift coefficient increased relative to the clean wing. The effects of the simulated ice shapes, located at 15% chord, on lift are shown in Fig. 20. It can be seen that although the lift curve slope was reduced for the iced cases, the stalling angle of attack and maximum lift coefficient increased.

Increases in lift coefficient at high angles of attack have been observed for spanwise-ridge ice accretions on airfoils. Whalen<sup>30</sup> and Papadakis et al.<sup>31</sup> investigated the effects of simulated spanwise-ridge ice accretions on airfoils at Reynolds numbers of  $1.8 \times 10^6$  and  $2.0 \times 10^6$ , respectively. They both observed that when the clean airfoil exhibited trailing-edge stall and the height of the ice simulation was comparable to the local boundary-layer thickness, the iced airfoil performed better at angles of attack near and above clean wing stall. This performance enhancement was attributed to the mixing layer generated by the ice shape entraining higher-momentum fluid into the boundary layer. This explanation may not suffice for the case of the ice simulations shown in Table 2. The size of these simulations ranged from 0.2-inches to 0.5-inches, likely making them significantly larger than the local boundary layer. It is also important to note that Broeren et al.<sup>32</sup>



**Fig. 20 Effect of simulated spanwise-ridge ice shapes located at 15% chord on GLC-305 swept wing,  $Re = 1.8 \times 10^6$ , after Papadakis et al.<sup>27</sup>**

showed that this lift enhancing effect on airfoils can be an artifact of low-Reynolds number testing of the clean airfoil. Their results showed that it is possible for the iced airfoil to have better high angle of attack performance characteristics than the clean airfoil at a Reynolds number of  $1.8 \times 10^6$ , but when compared to the clean airfoil at a Reynolds number of  $15.9 \times 10^6$  the iced airfoil performance degraded substantially. Due to these results it is difficult to determine the exact cause of the performance enhancement seen by Papadakis et al.<sup>27</sup> This also emphasizes the importance of investigating Reynolds number effects where such data are lacking.

Future research on spanwise ridge ice should explore Reynolds number effects. The authors are unaware of any swept-wing studies that used high-fidelity spanwise ridge ice shapes formed from castings of actual ice accretions. As a result, there are no data that can be used to validate the method of simulating ice shapes with simple geometries on swept wings. It is well known that real spanwise-ridge type ice accretion can be highly three dimensional with significant spanwise variation in the gross shape. Any future work must be supplemented with extensive flowfield studies in order to improve our understanding of how the ice accretions affect the aerodynamics of swept wings. Of particular interest is the spanwise vortex interaction with the spanwise ridge in determining the attendant aerodynamic effects.

### 3.0 SUMMARY

The continued design, certification and safe operation of swept-wing airplanes in icing conditions rely on the advancement of computational and experimental simulation methods for higher fidelity results over an increasing range of aircraft configurations and performance, and icing conditions. There is increasing demand to balance trade-offs in aircraft efficiency, cost and noise that tend to compete directly with allowable performance degradations over an increasing range of icing conditions. Aircraft icing research has now reached the level of maturity that computational methods and experimental tools are currently being used to address many of these challenges. However, knowledge gaps do remain for swept-wing geometries and larger droplet icing conditions. The current state-of-the-art in icing aerodynamics is mainly built upon a comprehensive understanding of 2D geometries developed from myriads of research efforts described in the technical literature. Such an understanding for fundamentally 3D geometries such as swept wings does not currently exist. The purpose of this report is to describe what is known of iced-swept-wing aerodynamics; to identify the type of research that is required to improve the current understanding; and to develop an aerodynamically based classification of swept-wing ice accretion. This report focuses on the fundamental aerodynamics of iced swept wings. The existing data tend to be: (1) mostly at low-Reynolds number and (2) applicable to simple swept-wing geometries that do not have high-lift systems, wing-mounted engines, fuselages and other features of actual airplane wings. These factors can significantly alter the iced aerodynamics for particular configurations and so extreme caution must be exercised in terms of making general conclusions based upon the current, limited database.

Ice accretion formations on swept wings can have unique characteristics. Depending upon specific icing conditions and sweep angle, the region of the attachment line may not be smooth as is often the case for airfoils. While initial roughness and rime ice accretion on swept wings tend to look very similar to that on airfoils, there can be significant differences for glaze ice accretion. For glaze icing, certain combinations of icing conditions and sweep angle can lead to the formation of highly 3D features called scallops that do not exist for ice accretions on airfoils. It is also possible to have glaze ice accretion with no scallops or even incomplete scallop formations on swept wings.

Following the method used in a previous review of iced-airfoil aerodynamics, this report classifies swept-wing ice accretion into four groups that are based upon unique flowfield features. Instead of relying upon ice accretion terminology such as rime and glaze, the four aerodynamic groups have names associated with ice-shape geometry. These four groups are: ice roughness, horn ice, streamwise ice and spanwise-ridge ice. This report attempts to describe the unique flowfield features of each group that determines the iced-wing aerodynamics:

- Ice roughness represents initial leading-edge ice accretion and a key aerodynamic characteristic is that the scale of the boundary-layer separation is of the same order as the size of the roughness. While there are many studies that have looked at roughness effects on swept-wing performance, including Reynolds number effects, there is a lack of flowfield data from which to interpret these results. More data are needed to understand the effects of roughness size, location and concentration on swept-wing aerodynamics.
- Horn ice is large, leading-edge ice accretion that can be associated with glaze icing conditions. The flowfield is characterized by large-scale, boundary-layer separation originating at the horn. This separation leads to the formation of a spanwise-running, leading-edge vortex that is similar to that found on clean

swept wings with leading-edge separation. There are a number of low-Reynolds number studies that have characterized the horn-ice flowfield for swept wings and documented the behavior of the leading-edge vortex preceding wing stall. This presents an excellent starting point, especially for nominally 3D horn shapes such as those with no scallops or even incomplete scallops. However, there are no flowfield data known to the authors for highly 3D horn ice such as complete scallop formations. Therefore, the fundamental aerodynamics are essentially unknown in this case. This is an important factor since the associated performance penalties may be large. The small amount of existing data indicate that there are fundamental flowfield differences between nominally 3D horn ice characterized by no scallop formations versus highly 3D horn ice characterized by fully developed scallop formations. Flowfield data, such as mean and fluctuating velocity profiles and surface shear stress are needed to further understand the important differences observed between these two cases of horn ice on swept wings.

- Streamwise ice can be associated with rime icing conditions and is generally conformal to the wing leading edge, or may form a horn-like feature (or protuberance) oriented into the flow direction. The only example of this group cited in this report showed an increase in wing maximum lift coefficient with the streamwise ice. While this effect may be possible, it is not expected to hold for most cases and illustrates the need for further wing performance data and flowfield information with realistic streamwise ice simulations.
- Spanwise-ridge ice can be associated with ice protection system operation in SLD icing conditions or incomplete evaporation of impinging water. The leading edge is free of ice with an ice ridge located downstream often in the range of 10 to 15% chord. This report describes data from only one low-Reynolds number study for very simple geometric representations of spanwise-ridge ice on a swept wing. More aerodynamic performance data and flowfield information are needed for realistic spanwise-ridge ice simulations.

For all of the proposed ice-shape classifications, relatively little is known about the 3D flowfield and even less about the effect of Reynolds number and Mach number on these flowfields. Both of these deficiencies are important and limit the ability to classify swept-wing ice accretion. Most of the data found in the literature pertain only to aerodynamic performance. Except for nominally 3D horn ice, flowfield information is limited to some pressure distributions, all at low-Reynolds number. Variations in Reynolds number found for iced-swept wings are all for relatively low-Reynolds number and provide no guidance as to the appropriateness of these data at Reynolds numbers approaching flight. In the 2D case, Reynolds and Mach number effects have been shown to be small in most cases and low-Reynolds number data have been used extensively to classify ice shapes and improve our understanding of iced-airfoil flowfields and aerodynamics. The very limited data available on swept wings to date suggest a similar result, but much more data are needed, particularly for realistic ice-shape simulations at higher Reynolds numbers.

The classifications and supporting data presented in this report can serve as a starting point as new research explores swept-wing aerodynamics with ice shapes. As further results become available, it is expected that these classifications will need to be revised just as has occurred in the airfoil case.

#### **Acknowledgements**

The authors would like to thank Joe Botalla at the University of Illinois who wrote the first draft of the literature review of swept wings with ice accretion and thus help initiate this paper. Abdi Khodadoust provided hard to acquire references from his extensive collection of icing papers. Several colleagues shared their expertise by reading a draft of this document and providing helpful comments and suggestions. This includes: Frederic Moens at ONERA; Cris Bosetti, Don Cook, Abdi Khodadoust, Adam Malone and Ben Paul at Boeing; Jim Riley at FAA; Sam Lee, Mark Potapczuk, Mary Wadel and Eric Kreeger at NASA Glenn. The authors from the University of Illinois were supported in this effort by a grant from the FAA Technical Center, DOT\_FAA 10-G-0004, with technical monitor Jim Riley. NASA's Atmospheric Environment Safety Technologies Project of the Aviation Safety Program also supported this work.

## References

- <sup>1</sup> Lynch, F.T., and Khodadoust, A., "Effects of Ice Accretions on Aircraft Aerodynamics," *Progress in Aerospace Sciences*, Vol. 37, No. 8, Nov. 2001, pp. 669-767.
- <sup>2</sup> Bragg, M.B., Broeren, A.P., and Blumenthal, L.A., "Iced-Airfoil Aerodynamics," *Progress in Aerospace Sciences*, Vol. 41, No. 5, Jul. 2005, pp. 323-362.
- <sup>3</sup> Broeren, A.P., Diebold, J.M. and Bragg, M.B., "Aerodynamic Classification of Swept-Wing Ice Accretion," NASA/TM – 2013-216381, 2013
- <sup>4</sup> Vargas, M., "Current Experimental Basis for Modeling Ice Accretions on Swept Wings," *Journal of Aircraft*, Vol. 44, No. 1, Jan.-Feb. 2007, pp. 274-290.
- <sup>5</sup> Anderson D. N. and Shin J., "Characterization of Ice Roughness from Simulated Icing Encounters," AIAA Paper 1997-0052.
- <sup>6</sup> Shin, J., "Characteristics of Surface Roughness Associated with Leading-Edge Ice Accretion," AIAA Paper 1994-0799.
- <sup>7</sup> Neely, R.H, and Connor, D.W., "Aerodynamic Characteristics of a 42° Swept-Back Wing With Aspect Ratio 4 and NACA 64<sub>1</sub>-112 Airfoil Sections at Reynolds Numbers From 1,700,000 to 9,500,000," NACA RM L7D14, 1947.
- <sup>8</sup> Kind, R.J., and Lawrysyn, M.A., "Effects of Frost on Wing Aerodynamics and Take-Off Performance," Paper 8 in "Effects of Adverse Weather on Aerodynamics," AGARD-CP-496, Dec. 1991.
- <sup>9</sup> Papadakis, M., Yeong, H.W., Chandrasekharan, R., Hinson, M., and Ratvasky, T.P., "Effects of Roughness on the Aerodynamic Performance of a Business Jet Tail," AIAA Paper 2002-0242, Jan. 2002.
- <sup>10</sup> Vargas, M., Papadakis, M., Potapczuk, M.G., Addy, H.E. Jr., Sheldon, D., and Giriunas, J., "Ice Accretions on a Swept GLC-305 Airfoil." SAE 02GAA-43, SAE General Aviation Technology Conference and Exhibition, Wichita, KS, Apr. 2002, Also NASA/TM-2002-211557, Apr. 2002.
- <sup>11</sup> Khodadoust, A. and Bragg, M.B., "Measured Aerodynamic Performance of a Swept Wing with a Simulated Ice Accretion," AIAA Paper 1990-0490.
- <sup>12</sup> Kwon, O.J., and Sankar, L.N., "Numerical Study of the Effects of Icing on Fixed and Rotary Wing Performance," AIAA Paper 91-0662, Jan. 1990.
- <sup>13</sup> Poll, D.I.A., "Spiral Vortex Flow Over a Swept-Back Wing," *Aeronautical Journal*, May 1986.
- <sup>14</sup> Bragg, M.B., Kerho, M.F., and Khodadoust, A., "LDV Flowfield Measurements on a Straight and Swept Wing with a Simulated Ice Accretion," AIAA Paper 93-0300, Jan. 1993.
- <sup>15</sup> Diebold, J.M, Monastero, M.C. and Bragg, M.B., "Aerodynamic of a Swept Wing with Ice Accretion at Low Reynolds Number," AIAA 2012-2795
- <sup>16</sup> Vassberg, J.C., DeHaan, M.A., Rivers, S.M. and Wahls, R.A., "Development of a Common Research Model for Applied CFD Validation Studies," AIAA 2008-6929
- <sup>17</sup> Diebold J.M. and Bragg, M.B., "Study of a Swept Wing with Leading-Edge Ice Using A Wake Survey Technique," To be presented at the 51<sup>st</sup> AIAA Aerospace Sciences Meeting, January 2013.
- <sup>18</sup> Brune, G. W., "Quantitative Low Speed Wake Surveys," *Journal of Aircraft* Vol. 31, No. 2, 1994.
- <sup>19</sup> Hoerner, S.F., Fluid-Dynamic Lift, Hoerner Fluid Dynamics, Brick Town, NJ, 1975.
- <sup>20</sup> Papadakis, M., Alansatan, S., and Yeong, H.W., "Aerodynamic Performance of a T-Tail with Simulated Ice Accretions," AIAA Paper 2000-0363, Jan. 2003.
- <sup>21</sup> Wright, W.B., "User's Manual for LEWICE Version 3.2," NASA/CR—2008-214255, Jan. 2008.
- <sup>22</sup> Busch, G.T., Broeren, A.P., and Bragg, M.B., "Aerodynamic Simulation of a Horn-Ice Accretion on a Subscale Model," AIAA Paper 2007-0087, Jan. 2007.
- <sup>23</sup> Papadakis, M., Gile-Laflin, B.E., Youssef, G.M., Ratvasky, T.P., "Aerodynamic Scaling Experiments With Simulated Ice Accretions," AIAA Paper 2001-0833, Jan. 2001.
- <sup>24</sup> Papadakis, M., Yeong, H.W., Wong, S.C., Vargas, M., and Potapczuk, M.G., "Aerodynamic Performance of a Swept Wing with Ice Accretions," AIAA Paper 2003-0731, Jan. 2003.
- <sup>25</sup> Papadakis, M., Yeong, H.W., Wong, S, Vargas, M and Potapczuk, M., "Experimental Investigation of Ice Accretion Effects on a Swept Wing," DOT/FAA/AR-05/39, Aug. 2005.
- <sup>26</sup> Bragg, M.B., and Gregorek, G.M., "Wind Tunnel Investigation of Airfoil Performance Degradation Due to Icing," AIAA Paper 82-0582, Jan. 1982.
- <sup>27</sup> Papadakis, M., Yeong, H.W., and Wong, S.C., "Aerodynamic Performance of a Swept Wing with Simulated Ice Shapes," AIAA Paper 2004-0734, Jan. 2004.
- <sup>28</sup> Busch, G.T, "Experimental Study of Full-Scale Iced-Airfoil Aerodynamic Performance Using Sub-Scale Simulations," Ph.D. Dissertation, Dept. of Aeronautical and Astronautical Engineering, Univ. of Illinois Urbana-Champaign, Urbana, IL, 2009.

<sup>29</sup> Lee, S. and Bragg, M.B., “Effects of Simulated-Spanwise Ice Shapes on Airfoils: Experimental Investigation,” AIAA Paper 99-0092, 1999

<sup>30</sup> Whalen, E.A. “Aerodynamics of Runback Ice Accretions,” Ph.D. Dissertation, Dept. of Aeronautical and Astronautical Engineering, Univ. of Illinois Urbana-Champaign, Urbana, IL, 2007.

<sup>31</sup> Papadakis, M., and Gile-Laflin, B.E., “Aerodynamic Performance of a Tail Section with Simulated Ice Shapes and Roughness,” AIAA Paper 2001-0539, Jan. 2001.

<sup>32</sup> Broeren, A.P., Whalen, E. A., Busch, G.T., and Bragg, M.B., “Aerodynamic Simulation of Runback Ice Accretion,” AIAA Paper 2009-4261, Jun. 2009.